Development of a Deep UV Resonance Raman Spectrometer

by

Jonathan D. Wert

B.S. Biochemistry, Muhlenberg College, 2009

Submitted to the Graduate Faculty of the

Kenneth P. Dietrich School of Arts and Sciences in partial fulfillment

of the requirements for the degree of

Master of Science

University of Pittsburgh

2014

UNIVERSITY OF PITTSBURGH

Dietrich School of Arts and Sciences

This thesis was presented

by

Jonathan D. Wert

It was defended on

April 17th, 2014

and approved by

Sunil Saxena, Professor, Department of Chemistry

Seth Horne, Assistant Professor, Department of Chemistry

Jeffry Madura, Professor, Department of Chemistry & Biochemistry, Duquesne University

Thesis Advisor: Sanford Asher, Distinguished Professor, Department of Chemistry

Development of a Deep UV Resonance Raman Spectrometer

Jonathan D. Wert, M.S.

University of Pittsburgh, 2014

UV resonance Raman spectroscopy is well-suited for studies of protein structure and dynamics due to its high sensitivity and selectivity. This has allowed for equilibrium as well as kinetic studies of protein folding, investigations of DNA-protein interactions, and characterization of explosive species.

This thesis is focused on a plan for the development of a deep UV resonance Raman spectrometer for excitation wavelengths from 197 nm – 240 nm. This spectrometer will utilize two gratings in a subtractive dispersion mode, giving a theoretical reciprocal linear dispersion of 0.424 nm/mm. This gives a theoretical limiting resolution of ~6 cm^{-1}. The gratings stages are equipped with motors, one of which drives a lead screw, and the other is a motorized linear actuator, which gives both stages high angular resolution. The stage controlled by the lead screw has sufficient resolution to shift the spectrum of a particular analyte by a single pixel. The expected efficiency of this spectrometer is ~15%, which is comparable to the efficiency of other double spectrometers. The development of this spectrometer will allow the continuation of incisive studies of protein and peptide structure.

TABLE OF CONTENTS

LIST OF FIGURES

1.0 INTRODUCTION

1.1 GENERAL USES OF UV RESONANCE RAMAN SPECTROSCOPY

UV resonance Raman spectroscopy (UVRR) was pioneered in the 1980s by the Asher and Spiro groups (1-6). It has since been used to study peptides and proteins in solution, high energy explosives such as TNT and RDX, characterizing bacteria, detecting polycyclic aromatic hydrocarbons, and characterizing chemically vapor deposited diamond-like films (7-16). The success of UVRR in studying a wide range of topics is due to the sensitivity and selectivity of the technique. This behavior derives from the fact that the environment of the molecule will many times affect the vibrational frequencies of its bands. For example, an amide group that is in an environment where it strongly hydrogen bonds with the solvent will have different vibrational frequencies than an amide group in an environment where it is not strongly hydrogen bonded to the solvent. Thus, this sensitivity can be used to probe the environment of UVRR chromophores. The selectivity derives from the selective enhancement of vibrations that are coupled to the electronic transitions in resonance with the excitation beam. For the peptide bonds in peptides and proteins, there is strong absorption ~200 nm. Thus excitation at ~200 nm allows for the selective monitoring of peptide bond conformation and environment (figure 1). A normal non-resonance Raman spectrum shows all of the Raman active vibrations of a molecule. In contrast, the UVRR spectrum is much less congested and allows for quantitative analysis (9, 10, 17-19).

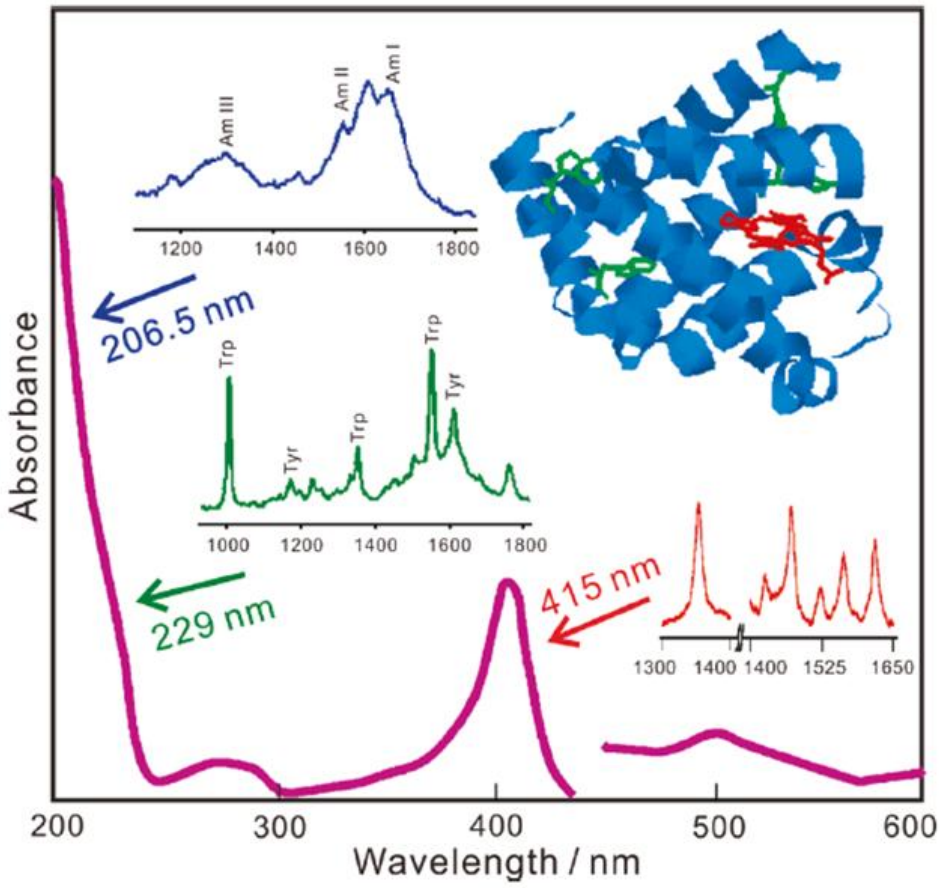

Figure 1. Absorption spectrum of myoglobin illustrating the selectivity of UV resonance Raman by tuning into different absorption bands of the protein. At 200 nm, the peptide bond vibrations are enhanced; at 229 nm the aromatic amino acid bands are enhanced; and at 415 nm, the heme group vibrations are enhanced. Reprinted with permission from (10), copyright 2012, American Chemical Society.

1.2 PEPTIDE/PROTEIN STUDIES BY UV RESONANCE RAMAN SPECTROSCOPY

Much of the pioneering work in UVRR has been geared towards the study of biomolecules. Protein folding is one of the long outstanding problems in biophysics. Given the

sensitivity and selectivity of UVRR for the amide protein and peptide bands, methods have been developed to determine the protein secondary structure, Ramachandran Ψ-angle distributions, and free energy landscapes from the UVRR spectrum (9, 10, 18-20). Chi et. al. (20) collected UVRR spectra of 13 different proteins of known crystal structures and calculated basis spectra for the α-helical, β-sheet, and unordered forms of the proteins. This allowed for the modeling of protein spectra with a linear combination of these three spectra to directly determine the secondary structure content of the protein directly from UVRR (20). In 2001, Asher et. al. (21) determined an empirical relationship between the Ramachandran Ψ-angle and the AmIII frequency. A plot of the AmIII frequency versus Ψ-angle revealed a sinusoidal relationship. It was also noticed that in more extended conformations the $C_\alpha H$ bending vibration was coupled to the AmIII, making this a spectroscopic marker for unordered content in peptides and proteins (21). Later, Mikhonin et al. confirmed the sinusoidal relationship with measurements of crystals of dipeptides with different Φ and Ψ-angles (22). Mikhonin et al. then further developed a series of equations for different secondary structure conformations of peptides in solution and was able to calculate the Ψ-angle distributions and free energy landscapes for peptides (17, 23).

Other studies have searched for markers for DNA-protein interactions, side chain environment, and monitored kinetics of peptide and protein folding with UVRR. Benevides et al. and Thomas have determined spectral markers for different forms and conformations of DNA, RNA, and markers for DNA interactions with proteins (24, 25). Huang et. al. have also conducted temperature jump studies on apomyoglobin to monitor the folding kinetics (26). They were able to monitor both aromatic amino acids such as phenylalanine and tyrosine as well as the amide bands with 197 nm excitation. They determined that in the unfolding of apomyoglobin that tertiary contacts of the core helices were lost first based on the faster response of a core

tryptophan residue than the amide of phenylalanine bands. Subsequently, the core helices melt (26). Mikhonin et. al. (23, 27) has conducted steady state and kinetic studies on a mainly polyalanine peptide AP that exists in a conformational equilibrium between α-helical and PPII conformations. They observed non-two state kinetics, and that the helical conformation actually consists of π-helices, 3_{10}-helices, and α-helices, which contribute to the non-two state folding kinetics (23, 27).

The Kim group has been able to apply UVRR to study the problem of membrane protein folding, further demonstrating the power of UVRR to study challenging systems (8, 28-30). Additionally, many UVRR studies on the environment of side chains have helped elucidate models for determining the conformations of these side chains in solution. For example, Tackeuchi et al. was able to determine a UVRR frequency model for the side chain dihedral angle for tryptophan and reproduce angles determined from protein crystal structures (31, 32). Hong et al. developed a model for the hydration of arginine in peptides based on model arginine compounds and was able to determine the average hydration state in these peptides (33).

1.3 SPECTROMETERS DEVELOPED FOR UV RESONANCE RAMAN SPECTROSCOPY

The above experiments would not have been possible without the development of instrumentation for the collection of deep UVRR spectra. A variety of UVRR spectrometers have been developed. The goal of any monochromator is to maximize the throughput and provide sufficient resolution to observe the Raman band of interest. This includes filtering the

Rayleigh scattered light and minimizing stray light that will decrease the signal-to-noise of the obtained Raman spectrum. Triple monochromamators were initially used in UVRR measurements to provide good Rayleigh scattered light rejection and stray light rejection (3). While these instruments had the advantage of limiting stray light and filtering out the Rayleigh scattered light in the spectrometer, the overall efficiency was extremely low in the deep UV (~3%) (3, 34).

Highly dispersive long focal length single-monochromators have also been used in more recent UVRR spectrometers. For example, Balakrishnan et al. employed a 1.26 m focal length spectrometer with a single 3600 groove/mm grating (35). Without a stage to filter the Rayleigh scattered light and reduce stray light, the overall signal-to-noise of single monochromators is generally lower than that of double monochromators. Variations on a double monochromator have also been employed by the groups of Kim and Mathies (8, 36). In their setup, a prefilter stage is used where a low dispersion prism is used to filter out the Rayleigh scattered light before the spectrograph stage disperses the light further (8, 36). This has the advantage of reducing stray light while still maintaining a higher throughput. They obtained about 50% throughput through this stage of the spectrometer (36). Conventional additive dispersion monochromators have been used as well (37). Additive dispersion double monochromators employ two gratings where both gratings disperse the light in the same direction. Thus, the stray light, which is the same frequency as the Rayleigh light, and Raman scattered light are dispersed in the same direction and the stray light will remain in the spectral region of interest. Bykov et al. designed a subtractive dispersion double monchromator where the first grating and the second grating dispersed the light in different directions, thus effectively dispersing the stray light out of the spectral region of interest (38). This is easily seen by comparing two spectrometers with

equivalent overall dispersions, but one employs additive dispersion and the other employs subtractive dispersion. In the case where a 600 groove/mm grating is used in first order for the first stage and a 2400 groove/mm grating is used in first order for the second stage, the equivalent dispersion is 3000 grooves/mm. The stray light in the spectrum is effectively dispersed by the 2400 groove/mm second grating. In the subtractive configuration, the second grating used is an 1800 groove/mm grating, but in the minus 2^{nd} order. The Raman light is dispersed effectively by a single 3000 groove/mm grating, but the stray light is dispersed by the equivalent of a 3600 groove/mm grating (figure 2) (38). Thus, for two double monchromators with the same overall equivalent dispersion for the Raman bands, the subtractive mode is better at eliminating the stray light since the second grating is more dispersive in the subtractive configuration. In the configuration described by Bykov et al. (38), relatively high resolution and high throughput was also maintained. The overall throughput for this spectrometer was ~20% in the 200-230 nm range of the spectrum, and the limiting resolution was 4.5 cm^{-1}. Compared to previous triple monochromators, the efficiency is ~7 times greater (3, 34, 38). Additionally, it allowed the collection of ~1500 cm^{-1} region of the spectrum of a peptide or protein, which is a large enough region to see all of the amide bands as well as internal standard bands.

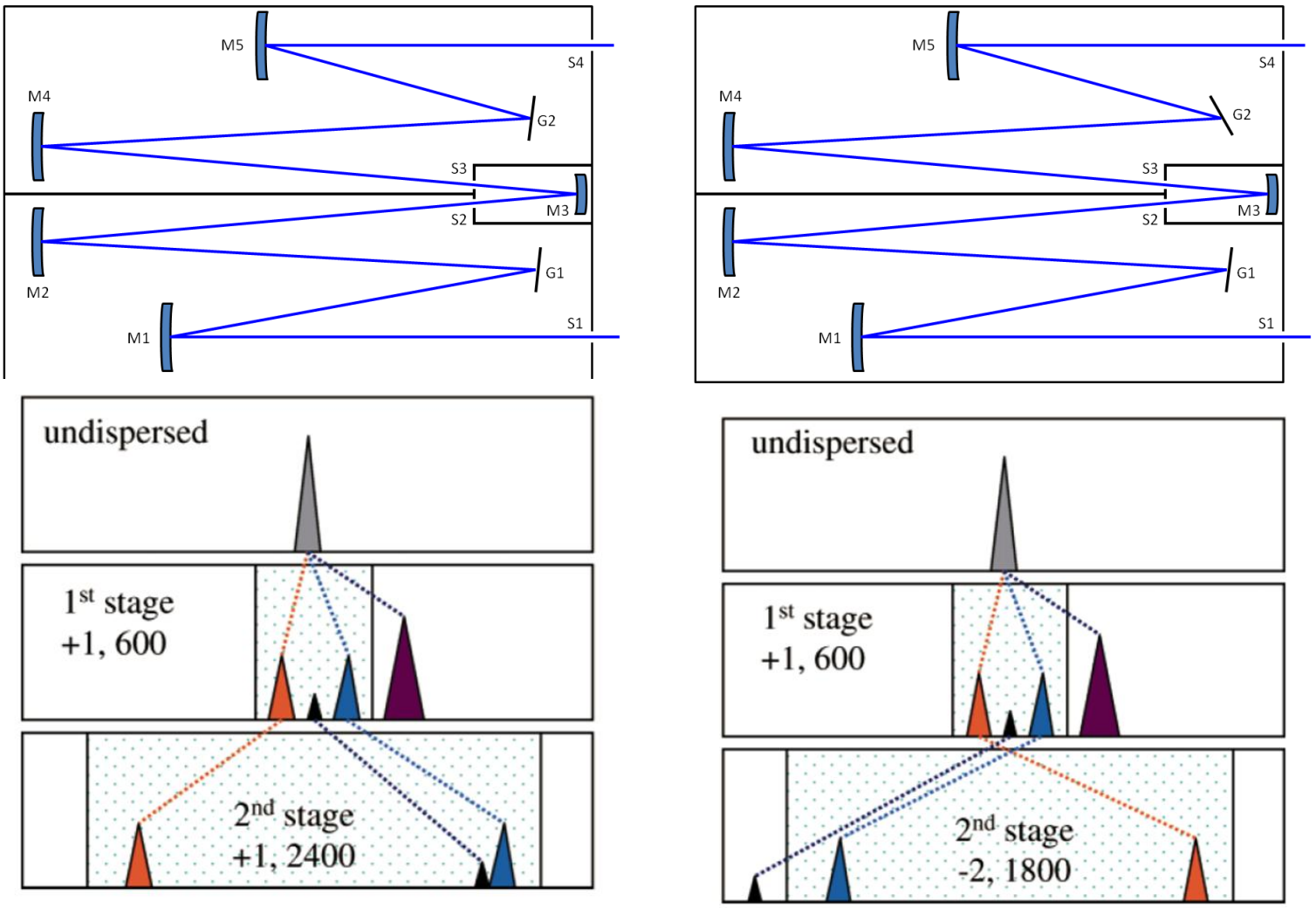

Figure 2. Left panel, top: Diagram of an additive dispersion double monochromator. The gratings disperse the light in the same direction. Left panel, bottom: Diagram of how the additive dispersion spectrometer disperses the light. Notice the stray light remains in the spectral region of interest. Right panel, top: Diagram of a subtractive dispersion double monochromator where the gratings disperse the light in opposite directions. Right panel, bottom: Diagram of how the subtractive dispersion spectrometer disperses the light. Notice now the stray light is out of the spectral region of interest, but the Raman bands switched sides. Bottom panels are from reference (38)

Recently, efforts have been made to increase the resolution of deep UVRR spectrometers, while maintaining a high throughput. The limiting factors again on increasing throughput and maintaining resolution are stray light rejection and Rayleigh light rejection. Bykov et. al. made

use of high order dispersion from an Echelle grating to accomplish this (34). The high order dispersion Echelle grating provided excellent stray light rejection and allowed the slit width to be 10 times greater than current spectrometers employed by the Asher group, while maintaining a resolution of 10 cm^{-1} (34). This allowed for the demonstration of a 0.84% spectral change in terms of peptide bond concentration. The downside of the Echelle grating spectrometer was the limited region of the spectrum that can be collected at the same time using conventional CCD cameras.

This thesis describes a plan for the development of a deep UVRR spectrometer that will use two grating stages in the subtractive dispersion configuration. Each grating stage will be motorized for easy movement to different excitation wavelengths. The resolution and efficiency are expected to be comparable to currently designed double monochromators. The grating stages should have enough resolution to move the spectrum of analyte a single pixel on the CCD camera.

2.0 DESIGN OF A DOUBLE MONOCHROMATOR FOR DEEP UV RESONANCE RAMAN SPECTROSCOPY

2.1 SPECTROMETER LAYOUT

The spectrometer being designed will be a modification of a SPEX 1403 double monochromater that was setup for additive dispersion with two 1800 groove/mm gratings. For our system, the gratings were decoupled by removing the mechanical metal attachment between the two rotating mounts for use in subtractive dispersion mode. As discussed above, this subtractive mode allows for the minimization of stray light that reaches the detector. The stage for the first grating was equipped for control with a linear actuator (TRA25CC, Newport, Inc.) that has a 25.4 mm range of travel and is controlled by a CONEX controller. The minimum incremental motion of this actuator is 0.2 microns. A 17.5 cm metal bar was attached to the rotating axis of the grating mount. The actuator pushes on a brass cylindrical rod that is slotted into the metal bar to rotate the grating. The stage for the second grating was equipped to be controlled with a stepper motor that turns a precise lead screw to rotate the grating (figure 3). The lead screw step size was given in the manual to be 0.0025 cm^{-1} for the 1800 groove/mm grating set configured in additive dispersion. This step size is based on the dispersion of the spectrometer a 514.5 nm, the wavelength used by SPEX to characterize the spectrometer. In the original design of the spectrometer (two 1800 groove/mm gratings mechanically coupled in

additive dispersion), the drive for the lead screw was designed to be linear with respect to excitation wavenumber. Thus, the spectrometer drive for the lead screw will have to be recalibrated since the gratings were decoupled. Both gratings have the capability to be individually computer controlled with simple commands. The stage for the second grating can also be controlled with a simple custom designed controller that controls the stepper motor (described more in section 2.9). The spectrometer base plate also is temperature controlled, which allows for the elimination of moisture buildup in the spectrometer and on the optics. The temperature is set to 29.6°C.

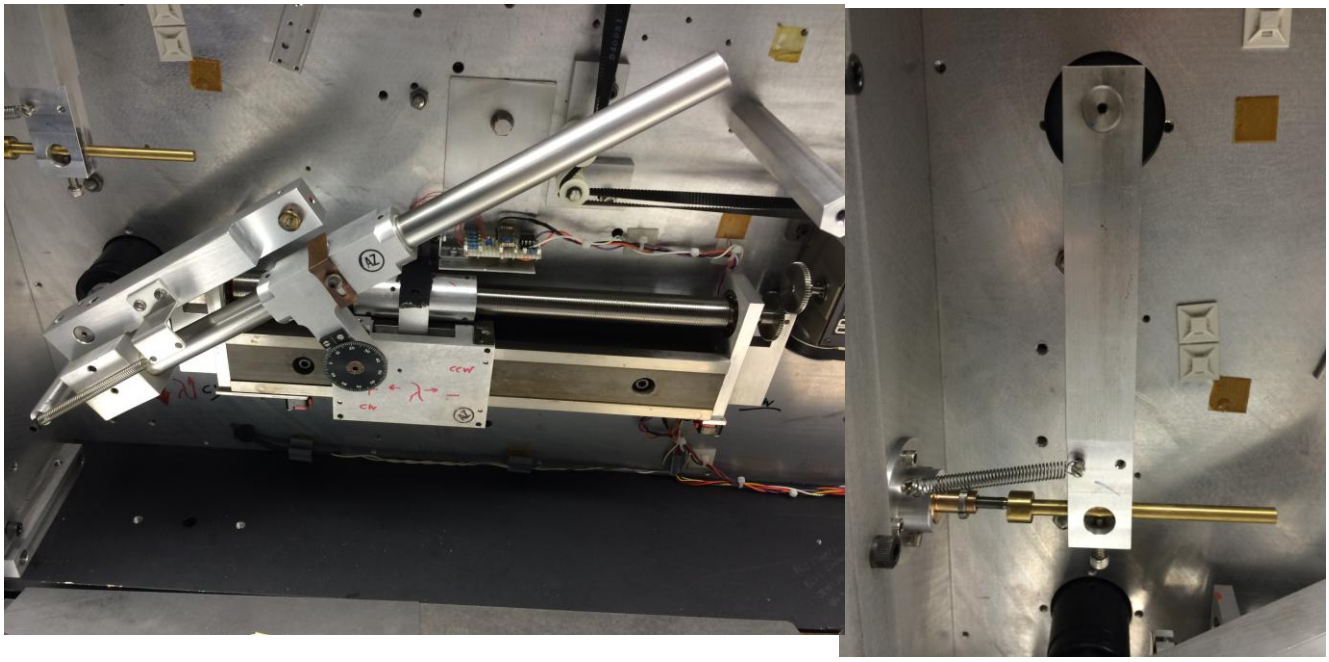

Figure 3. Picture of the lead screw (left) that controls grating 2 and the actuator that pushes on a 17.5 cm metal bar (right) that controls grating 1. Both are motor controlled.

The spectrometer has the layout described in figure 4. The scattered light from the sample is focused onto the entrance slit, S1, and collimated by M1. G1 then disperses the light and M2 focuses the dispersed light through the middle slit, S2, to M3, which focuses the light through the second middle slit, S3. M4 then collects and collimates the light and directs it to G2,

where it is dispersed onto M4 and focused onto the detector. The mirrors used in this spectrometer are 5 inch aluminum mirrors with a dielectric coating, which has ~94% reflection in the region of 197 nm – 241 nm (figure 5). The focal lengths of the mirrors are 84 cm. The effective diameter of the mirror is 4 inches, which matches the 4″ x 4″ area of the grating. The first grating, G1, used as the filter stage is a 1000 groove/mm magnesium fluoride coated holographic grating with a blaze wavelength of 230 nm. This grating will be used in the first order. The second grating is a 1800 groove/mm magnesium fluoride coated plane ruled grating with a blaze wavelength of 409.18 nm and blaze angle of 21.10°. This grating will be used in minus second order. The middle slits in the original SPEX 1403 spectrometer contained 25 cm focal length lenses to transfer the slit image from one "single" monochromator of the double to the other "single" monochromator. These lenses were replaced with 25 cm UV fused silica lenses from CVI with a 193 nm antireflection coating. This antireflection coating allows ~98% transmission in the spectral region of 193 nm – 240 nm.

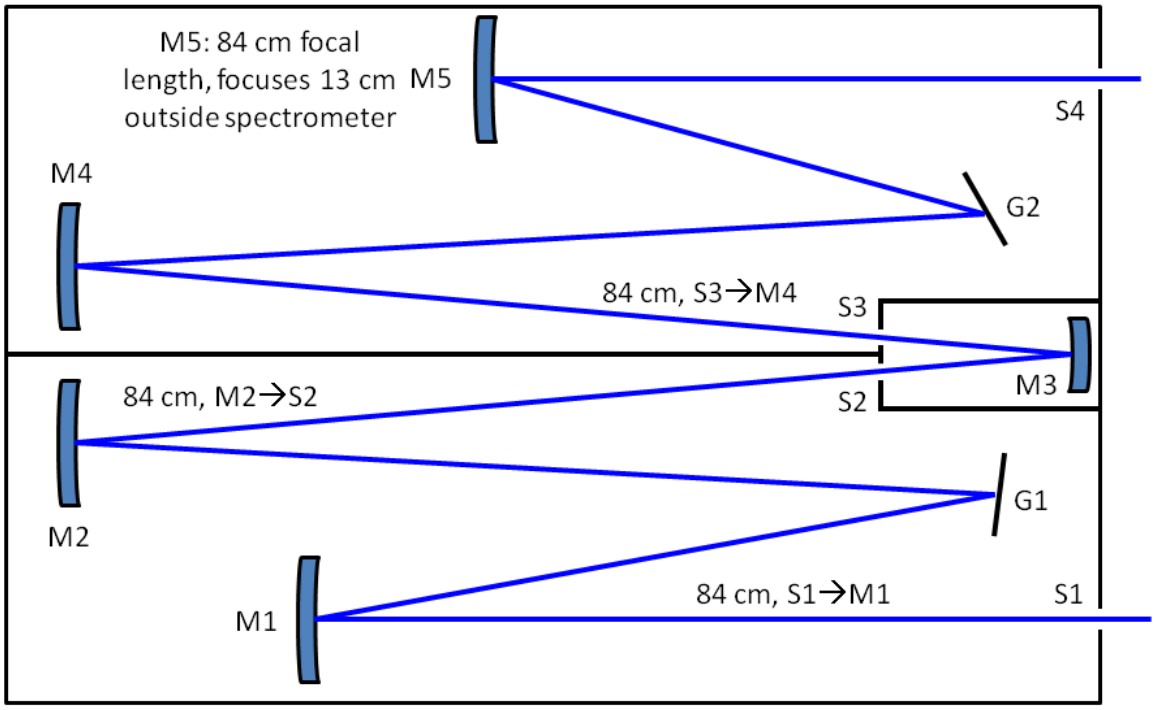

Figure 4. Schematic of SPEX 1403 double monochromator in the subtractive configuration. The mirrors have 84 cm focal lengths except for M3, which has an 11 cm focal length. The first grating is 1000 grooves/mm and used in first order and the second is 1800 grooves/mm and used in the minus second order.

The detector used in this spectrometer will be a Roper Scientific Pylon liquid nitrogen cooled CCD camera. This camera is specified by the manufacturer to have a quantum efficiency of ~35% down to 250 nm. This camera has been used for other spectrometers in the Asher group, so we are confident that this will be the best choice of detector (34, 38). Additionally, the previous instrument designed by Bykov et. al. (38), utilized another CCD camera from Roper Scientific, the Spec10:400B, which has given us great success in obtaining UVRR spectra over the past 10 years.

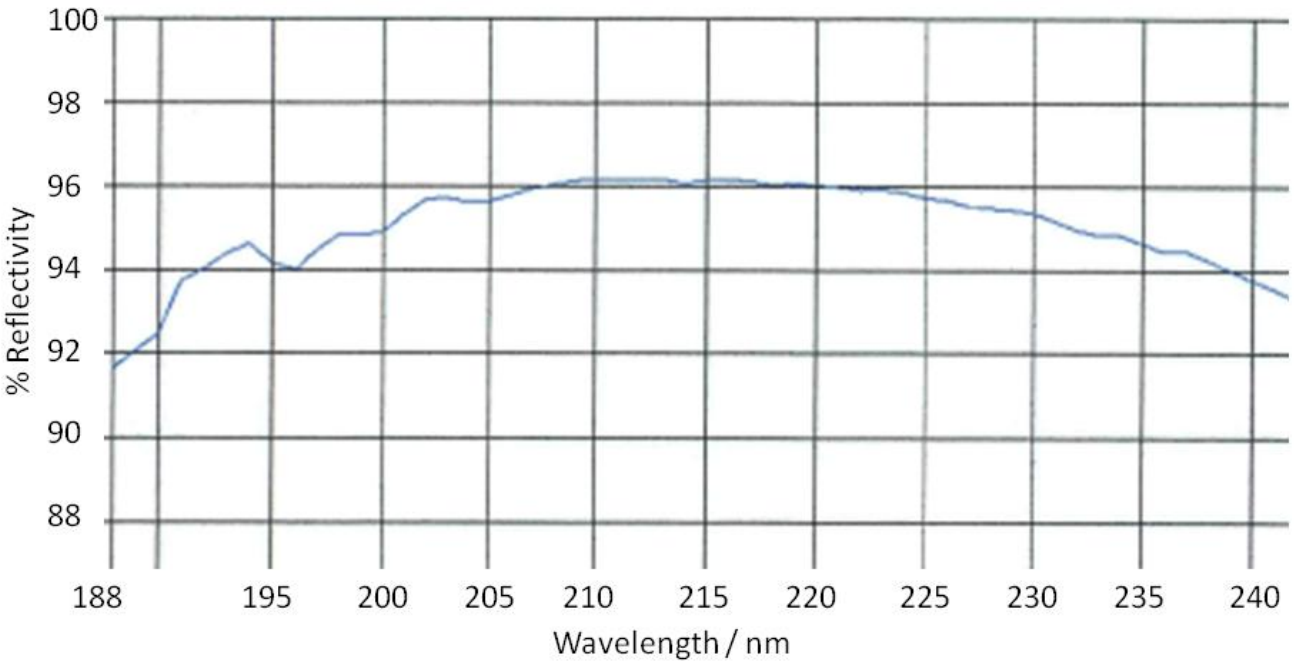

Figure 5. Reflectivity curve for the mirror coatings demonstrating the >94% reflectivity in the 197-241 nm region. The coating is a dielectric coating and the mirrors were coated by Applied Research Optics (formerly owned by Saint-Gobain, Inc.).

2.2 DISPERSION AND RESOLUTION

2.2.1 Reciprocal Linear Dispersion

The dispersion of the spectrometer and the focal length determine the resolution that is attainable. To calculate the dispersion and resolution, it is useful to think of the grating combination as an "equivalent" singe monochromator operated in first order (figure 6). The system being designed will have dispersion that is equivalent to a single 2600 groove/mm grating. The value Φ describes the angle between the grating axis and the mirrors. This angle is fixed based on the spectrometer geometry and for our system is 5.23 degrees. The angle θ is the

angle between the grating axis and the grating normal and is dependent on the wavelength of light diffracted by the grating. For the equivalent grating system, θ is the difference in magnitude of the θ angles for each "single" monochromator of the double monochromator since our gratings are arranged in the subtractive dispersion mode. For our system, the equivalent θ angle is 15.13 degrees for 200 nm light. This equivalent θ angle can also be calculated using the grating equation, $2d\sin\theta\cos\Phi = m\lambda$, and the calculated Φ angle. The angles α and β are needed to calculate the reciprocal angular and reciprocal linear dispersions. α is defined as the angle between the grating normal and the incident beam, and thus equivalent to θ minus Φ. For our configuration, α is 9.90 degrees. β is defined as the angle between the grating normal and the exit beam, and thus equivalent to θ plus Φ. The reciprocal angular dispersion is given by $R_a = \frac{\lambda \cos\beta}{\sin\alpha + \sin\beta}$ and calculated to be 360.6 nm/rad. The reciprocal linear dispersion is given by $R_d = \frac{\lambda \cos\beta}{f(\sin\alpha + \sin\beta)}$ and calculated to be 0.424 nm/mm. For 200 nm light, this corresponds to 106 cm^{-1}/mm and 2.12 cm^{-1}/pixel (using the CCD camera pixel width of 20 microns).

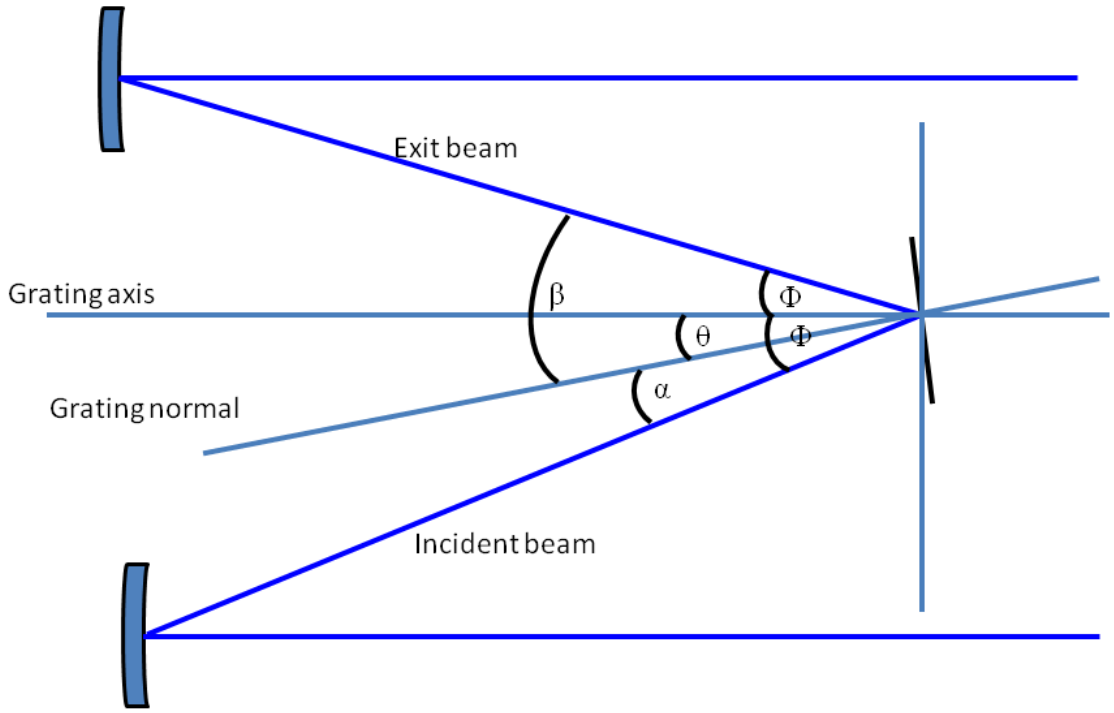

Figure 6. Schematic of the "equivalent" single monochomator derived from the double monochromator in figure 4.

2.2.2 Limiting Resolution

The limiting resolution of the spectrometer can be theoretically calculated based on the reciprocal linear dispersion in cm^{-1}/mm, the pixel width, and the number of pixels needed to resolve two bands; the equation is given by, $\text{limiting resolution} = R_d \times P_w \times 3 \text{ pixels}$. If we assume that a minimum number of three pixels is needed to resolve two bands, the limiting resolution will be 6.4 cm^{-1}. If a 100 micron slit width is used, the image on the camera will cover 5 pixels. Thus, the width a Raman band will be ~10 cm^{-1}.

2.3 ANGULAR RESOLUTION OF GRATING STAGES

The angular resolution of the grating stages will allow us to test for the possibility of shifting the spectrum of the analyte of interest by a single pixel. For G1, the filter stage grating is controlled by a linear actuator with a minimum step size of 0.2 microns. This actuator pushes on a metal rod slotted into a 17.5 cm metal bar attached to the rotation axis of the grating. Assuming we take one step with this actuator, the minimum angular resolution of the grating mount can be determined. Since the step size is very small, the angle the stage is rotated is equivalent to the inverse tangent of the step size divided by the length of the metal bar. This gives a minimum angular resolution of 6.6×10^{-5} degrees for the grating stage (figure 7).

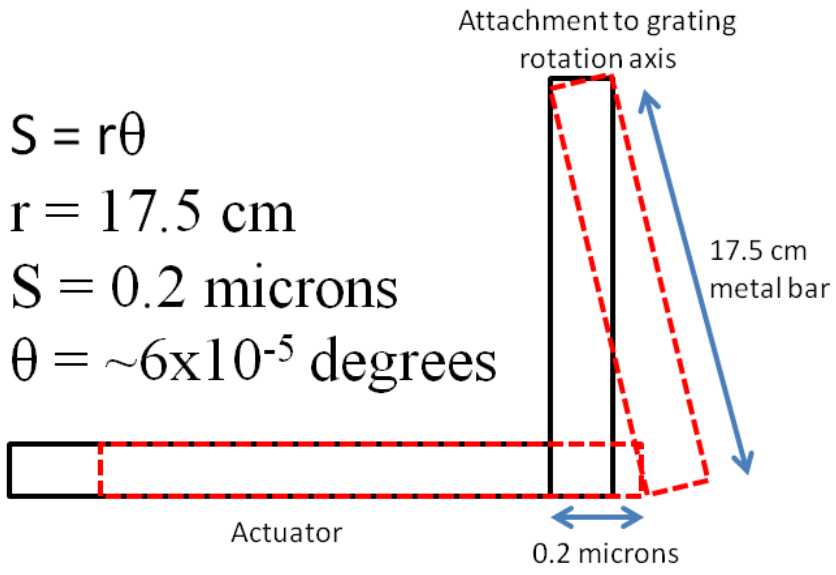

Figure 7. Diagram of the determination of the angular resolution of the grating stage controlled b the actuator. The angle rotated can be estimated from the arc length of a minimum step, which is 0.2 microns. An angle of $\sim 6 \times 10^{-5}$ degrees is the angular resolution of the grating stage.

For G2, the spectrograph stage grating, the angular resolution can only be estimated from the specifications of the mirrors and gratings given in the documentation for the spectrometer. The original SPEX 1403 spectrometer had two 1800 groove/mm gratings coupled in additive dispersion. At 514.5 nm, this gave a minimum drive step of 0.0025 cm^{-1}. If we take the minimum wavenumber step, given that the specified reciprocal linear dispersion is 12.5 cm^{-1}/mm, the step taken is equivalent to 0.2 microns, or 1/100 of the pixel width. Even if we assume that the step size is only 0.1 cm^{-1} at 200 nm, which is 100 times smaller than the step size at 514.5 nm, the step size taken is 0.95 microns, or 1/20 of the pixel width. This gives us confidence that moving this grating will certainly allow the spectrum of a sample to be moved a single pixel on the CCD chip. The degrees of rotation necessary to move the spectrum a single pixel can be estimated from the inverse tangent of the pixel width over the focal length, assuming the dispersion does not change by moving such a small increment. This angle is estimated to be 0.0013 degrees for a 20 micron pixel width and an 84 cm focal length mirror. The angular precision of the lead screw can be estimated by taking the minimum wavenumber step size of the lead screw and dividing by the angular dispersion of that stage. If the angular dispersion of the spectrograph stage is 2334 cm^{-1}/deg at 200 nm, and the minimum wavenumber step size is 0.1 cm^{-1}, the angular precision of the lead screw is 4.3×10^{-5} degrees, which is more than enough to move the spectrum of a sample a single pixel on the CCD camera.

2.4 DESCRIPTION OF THE COLLECTION OPTICS

To obtain maximum signal, we need to be able to collect and disperse as much scattered light as possible, while still maintaining a setup that is experimentally tractable. The current

double monochromator described by Bykov et al. (38), utilizes a 10 cm focal length, two-inch lens to collect the Raman scattered light. In the setup described here, we wish to decrease the focal length of that lens in order to collect more light. The focal length of the lens we will use to collect and collimate the light is 7.5 cm and two inches in diameter. This allows the solid angle collected to be increased by a factor of ~1.7 (for the 10 cm lens, $\Omega = 0.19$ sr, for the 7.5 cm lens, $\Omega = 0.33$ sr). The second lens is f-matched to the first spectrometer mirror to collect as much light as possible. Since the mirrors in the spectrometer have a focal length of 84 cm and a diameter of four inches, the focal length of the second two-inch lens needs to be ~42 cm. This lens combination gives a magnification of about 5.6 on the spectrometer entrance slit. Thus for a 200 micron excitation beam size, the spot on the slit will be approximately 1.1 mm.

2.5 SPECTROMETER EFFICIENCY

The theoretical efficiency of the spectrometer can be calculated based on the efficiency of all of the components in the system. This includes 5 mirrors, two gratings, and two lenses in the middle slits. The mirrors have ~94% reflectivity in the region of 197 nm – 241 nm. The lenses have 98% transmission in the same region. The 1000 groove/mm holographic grating has an efficiency of ~40% in the first order at 204 nm. The 1800 groove/mm grating has an efficiency of ~50% in the 2^{nd} order. The overall calculated efficiency is the product of the efficiencies of all of the components of the system. This theoretical efficiency is calculated to be ~15%. This is comparable to the efficiency of the current double monochromator which is ~20% efficient (38), and much better than that of our triple monochromator, which is ~3% efficient (3, 34).

The efficiency of the spectrometer will be experimentally measured after alignment. A barium sulfate white reflectance standard that has almost 100% scattering in the deep UV will be used (39). The $BaSO_4$ surface will be illuminated by a standard deuterium lamp and efficiency curves will be collected at a variety of wavelength settings between 200 nm and 240 nm. The curves will be collected in the following manner: set the gratings, collect a spectrum, collect a wavelength spectrum with the standard lamps for calibration, and then move the grating settings to a new wavelength and repeat the process. Zinc and cadmium lamps will be used to calibrate the efficiency curves to wavelength. The use of zinc and cadmium standard lamps will also allow calibration of the motorized grating drives for the spectrometer. Zinc has emission wavelengths at 202.5, 206.2, and 213.9 nm. Cadmium has emission wavelengths at 214.4, 226.5, and 228.8 nm. If necessary, the Positive Light Indigo-S 210 nm – 240 nm tunable Ti:Sa laser can be used for longer wavelength calibration. Also, the new deep UV 213 nm laser from UVisIR can be used if necessary. The efficiency curves will then be normalized to the measured throughput of a 229 nm laser beam in order to determine the absolute efficiency as a function of wavelength.

2.6 MEASUREMENT OF INSTRUMENT FUNCTION

For an ideal spectrometer with perfect optics, perfect alignment, and no effect from the entrance slit, the observed bandshape of a Gaussian laser beam that passes through spectrometer will be Gaussian. However, the optics are never perfect, and there is an effect of illuminating the entrance slit on the spectral bandshape. It is important to characterize this effect. The observed bandshape of a Gaussian laser beam that passes through the spectrometer will be a convolution

of the laser beam frequency bandshape and the spectrometer instrument function. To measure the effect of the entrance slit on the laser beam bandshape, spectra will be collected at a range of slit widths from 10 microns to 300 microns and plotted versus the FWHM of the laser beam. Extrapolation to zero slit width will tell us the effect of the slit on the spectrum.

It will also be useful at this point to compare the FWHM of the Teflon® 1379 cm^{-1} band to the FWHM of the band with the current double monochromator described by Bykov et. al. It is observed, with good spectrometer alignment, CCD camera alignment, and a 100 micron slit width, the FWHM of the 1379 cm^{-1} Teflon® band is ~9-10 pixels (figure 8). In practice, when the camera is being aligned, the width of this band is estimated by counting the number of pixels on each side of the maximum peak frequency of the 1379 cm^{-1} Teflon® band.

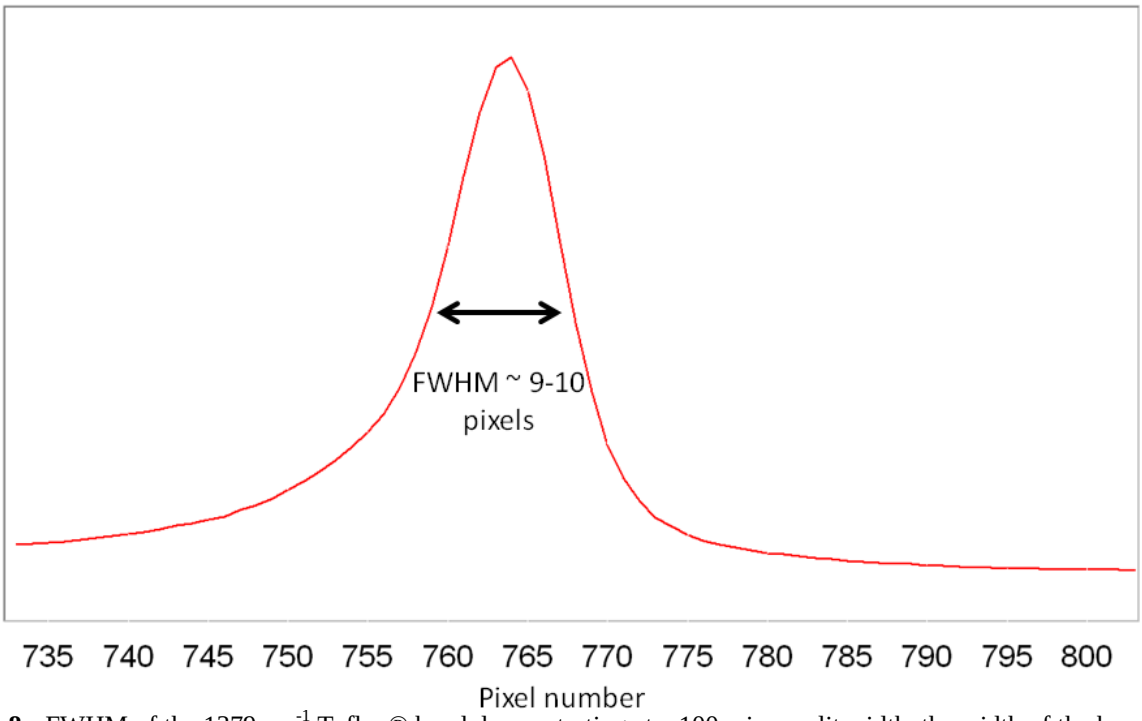

Figure 8. FWHM of the 1379 cm^{-1} Teflon® band demonstrating at a 100 micron slit width, the width of the band is ~9-10 pixels. Measuring the width of Teflon® will confirm good camera alignment and spectrometer alignment. The width was measured by counting the number of pixels on either side of the peak frequency maximum of the

1379 cm^{-1} Teflon® band. This spectrum was measured with 204 nm excitation on our current double monochromator described by Bykov et al. (38). The total accumulation time was 9 seconds.

2.7 EXPERIMENTAL CONFIRMATION OF THE RECIPROCAL LINEAR DISPERSION

In section 2.2, the reciprocal linear dispersion was estimated based on the calculated θ, Φ, α, and β angles for the dispersion of 200 nm light on the gratings. We plan to experimentally confirm the calculated reciprocal linear dispersion, and from that, our new calculated limiting resolution.

We will accomplish this by collecting spectra of calibration standards, such as Teflon®, cyclohexane, and acetonitrile in which the Raman shift frequencies are well characterized. Teflon® has two bands in our spectral region of interest at 732 cm^{-1} and 1379 cm^{-1} (40). Acetonitrile also has two bands ~918 cm^{-1} and 1376 cm^{-1} (43). Cyclohexane has bands across the entire spectral region of interest ~802 cm^{-1}, ~1027 cm^{-1}, ~1157 cm^{-1}, ~1266 cm^{-1}, ~1347 cm^{-1}, ~1443 cm^{-1}, and ~1465 cm^{-1} (43). We will then determine the reciprocal linear dispersion by comparing two bands and the number of pixels between each band from farther apart regions of the spectrum. The ratio of the wavenumber difference in frequency over the pixel difference will give an experimental estimated measure of the reciprocal linear dispersion. Figure 9 demonstrates this for the double monochromator described by Bykov et al. using Teflon® (38).

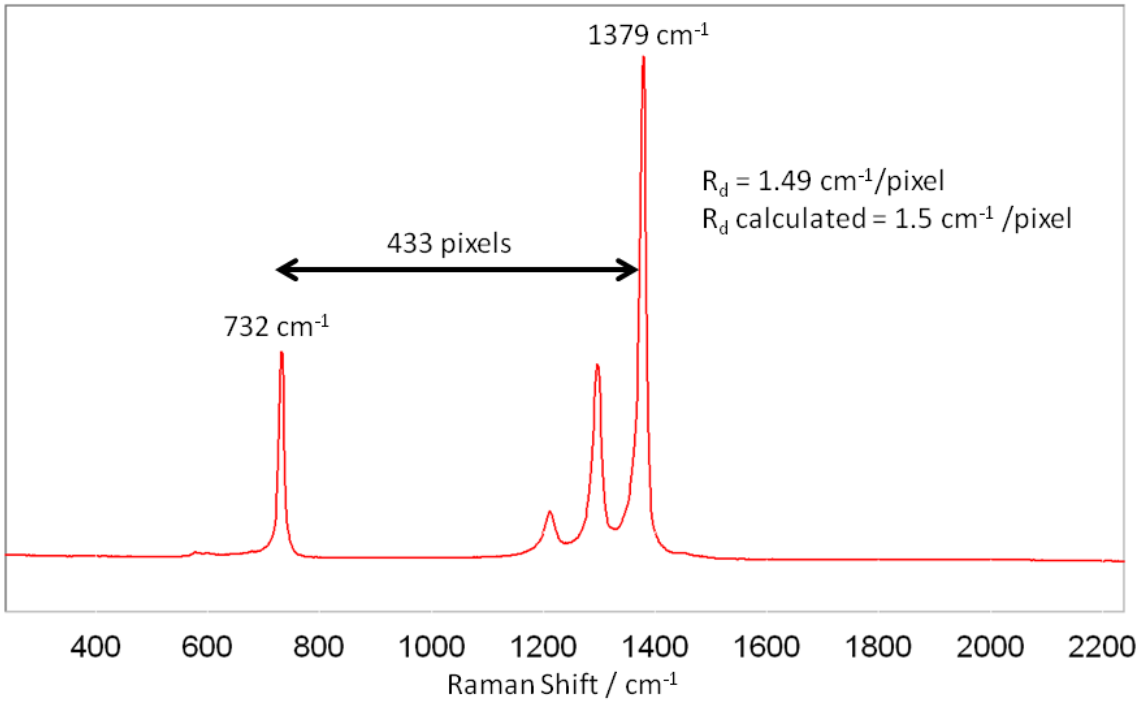

Figure 9. FWHM of the 1379 cm^{-1} Teflon® band demonstrating at a 100 micron slit width, the width of the band is ~9-10 pixels. Measuring the width of Teflon® will confirm good camera alignment and spectrometer alignment. The width was measured by counting the number of pixels on either side of the peak frequency maximum of the 1379 cm^{-1} Teflon® band. This spectrum was measured with 204 nm excitation on our current double monochromator described by Bykov et al. (38). The total accumulation time was 9 seconds.

2.8 EXPERIMENTAL CONFIRMATION OF SINGLE PIXEL ANGULAR RESOLUTION

In section 2.3, the angular resolution of the gratings was discussed. It was concluded that theoretically the lead screw and linear actuator that control the grating mounts would have enough angular resolution to shift the spectrum of a sample by a single pixel. We plan to experimentally confirm this.

To experimentally confirm that we can shift the spectrum of a sample by single pixel, we will collect a spectrum of Teflon®; then we will move the second grating stage an angle of 0.0013 degrees, since this was the theoretical angle change that would move the spectrum a single pixel, and collect another spectrum. The exact numbers on the wavelength readout attached to the lead screw drive that will accomplish this movement will be determined once the spectrometer is calibrated. The spectrum will then be moved back to the original spot to determine if any major backlash or hysteresis is occurring in the drive for the lead screw.

2.9 CONTROL OF GRATING STAGES

Both grating stages are motor controlled. The second grating is attached to a lead screw that is rotated by a stepper motor (see figure 3). The stepper motor also turns a dial that reports the wavenumber on the outside panel of the spectrometer. The stepper motor can be controlled one of two ways: 1) With a custom controller designed by the University of Pittsburgh electronics shop; 2) With the software Si Programmer™. The custom controller was equipped with buttons that rotate the stepper motor clockwise or counter-clockwise, which then rotates the lead screw. This is the easiest way to control the grating and will be used most often in practice to rotate the grating. Once the spectrometer is re-calibrated, the wavenumber reading on the outside panel of the spectrometer will allow easy tuning of the grating to different excitation wavelengths.

The Si Programmer™ software can also be used to control the grating. The software interface consists of a list of command lines where different software built in commands can be entered. Clicking on a line number opens an interface with commands that the user can send to

the motor. The most useful command is the "feed to length" command, which allows the user to enter the number of steps they want the motor to take, the speed, the acceleration and deceleration of the motor, and whether the motor is to move clockwise or counter-clockwise. Once the spectrometer is calibrated, the number of motor steps will be related to the wavenumber reading on the side panel of the spectrometer and the number of steps to move between wavelengths can easily be entered.

An actuator that pushes on a metal bar attached to the rotation axis of the grating stage controls the first grating (see figure 3). This actuator is controlled by a CONEX-CC controller applet, which is run through a program called NSTRUCT. The user interface of the applet allows the user to enter a position from zero to 25 mm in the "target motion/PA-absolute move" box. This will be the easiest way to move the grating. Once the spectrometer is calibrated, the exact position of the actuator can be related to the excitation wavelength. The minimum step size of the actuator is 0.2 microns.

3.0 MEASUREMENT OF UV RESONANCE RAMAN SPECTRA OF PEPTIDES AND PROTEINS

3.1 EXPERIMENTAL SETUP

The excitation wavelength used for the measurement of UVRR spectra of peptides and proteins will be 204 nm. This wavelength is in resonance with the peptide bond deep UV electronic transitions.

The 204 nm light is either obtained frequency doubling, tripling, and then wave mixing the fundamental a Ti:Sa laser operating at a 1 kHz repetition rate or by Raman shifting ~1.6 W of 355 nm light from the 3rd harmonic of an Nd:YAG laser operating at 100 Hz repetition rate in ~30 psi hydrogen gas and separating the 5th anti-stokes beam with a Pellin-Broca prism. Generally, from both of these processes about 2-3 mW of power is obtained, which is enough to record high S/N UVRR spectra. The 204 nm light is focused by a one inch diameter lens and reflected onto the sample by a prism at an angle of ~165 degrees (with respect to the optical axis of the collimating lens described above). The scattered light from the sample is then collected by the collimating lens (described above) and focused into the spectrometer, where it is dispersed and collected by a liquid nitrogen cooled CCD camera. Figure 10 shows a general schematic of the setup.

For peptides, a flow cell has been designed where the solution recirculates through the flow cell with a gear pump. The flow cell has been previously described by Bykov et. al. (38) to consist of a brass casing with an enclosed 200 mm stainless steel tube with a diameter of 0.6 mm. For proteins, a setup where the solution is pumped from a syringe pump through a capillary tube is available that is gentler on the protein sample of interest than the gear pump and flow cell used for peptide samples (20).

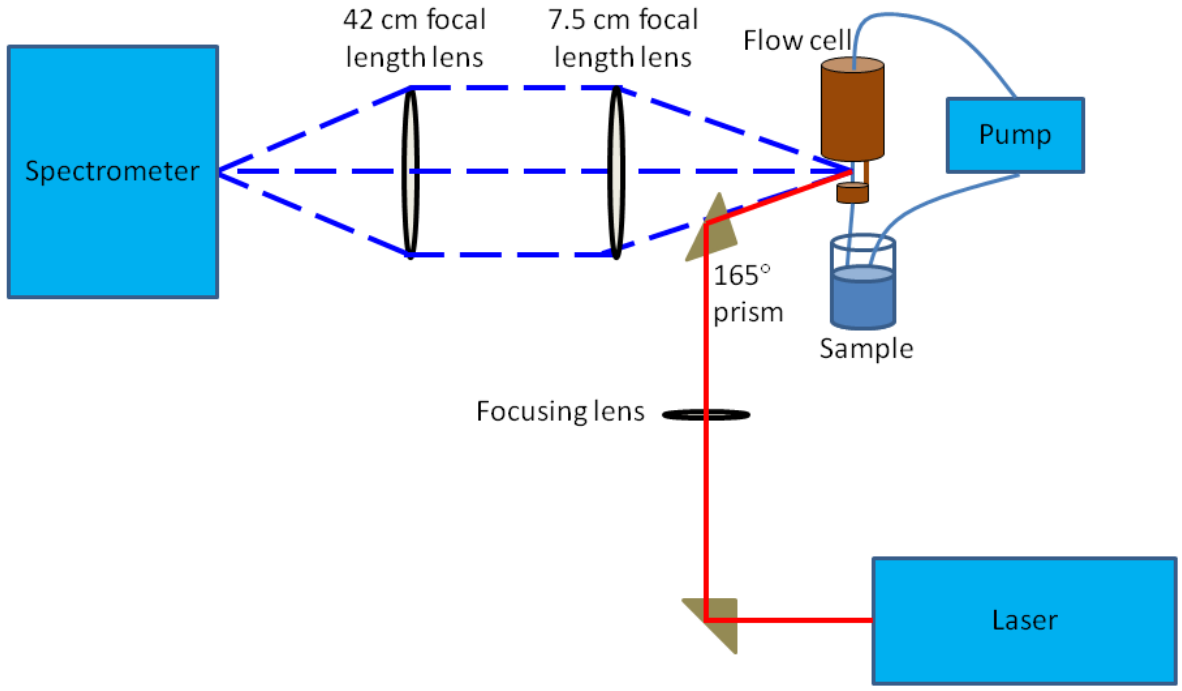

Figure 10. General setup of the UV Raman instrumentation. The 204 nm beam exits the laser, either from the Ti:Sa or the Nd:YAG system, passes through a focusing lens where it is focused to the sample. A 165 degree backscattering geometry is used. For peptides a flow cell recirculates the sample through the excitation beam. The scattered light is collected by a 7.5 cm focal length collimating lens and then focused into the spectrometer by a 42 cm focal length lens where it is dispersed and detected by a CCD camera.

3.2 MEASUREMENT OF TRIALANINE AS A TEST

UVRR spectra of trialanine will be collected as a test of this spectrometer. Trialanine is a simple peptide system that exists in an extended conformation and does not aggregate (41). We should expect to see bands for the AmIII, AmII, AmI, $C_\alpha H$ bending, and methyl group motions for the alanine side chain. The AmIII is expected to be broad and have a maximum ~1266 cm^{-1}; the AmII is expected to occur ~1550 cm^{-1}, and the AmI is expected to occur ~1655 cm^{-1}. The $C_\alpha H$ bending has bands ~1330 cm^{-1}, ~1370 cm^{-1}, and ~1390 cm^{-1} and these overlap with the CH_3 motions of the alanine side chain (42) (figure 11).

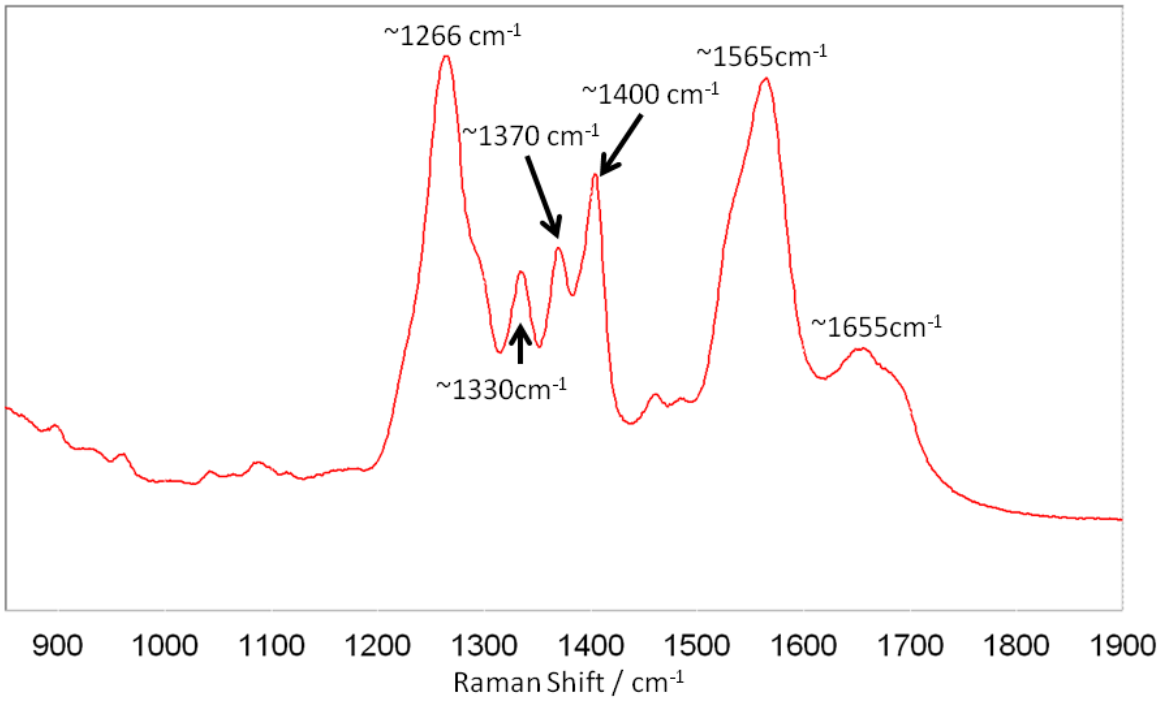

Figure 11. Sample spectrum of trialanine in water showing the AmIII band (~1266 cm^{-1}), the AmII band (~1565 cm^{-1}), the AmI band (1655 cm^{-1}), and bands due to CαH bending and methyl group motions (~1330 cm^{-1}, ~1370 cm^{-1}, shoulder ~1390 cm^{-1} not shown). The carboxylate stretch is ~1400 cm^{-1}. This spectrum was measured with 204 nm excitation using our current double monochromator described by Bykov et al. (38). The concentration of

trialanine was 1 mg/mL and the total accumulation time was 50 minutes. Water was not subtracted from this spectrum.

BIBLIOGRAPHY

1. Asher SA. UV Resonance Raman Studies of Molecular Structure and Dynamics: Applications in Physical and Biophysical Chemistry. Annual Review of Physical Chemistry. 1988;39(1):537-88.
2. Asher SA. UV resonance Raman spectroscopy for analytical, physical, and biophysical chemistry. Part 1. Analytical Chemistry. 1993;65(2):59A-66A.
3. Asher SA, Johnson CR, Murtaugh J. Development of a new UV resonance Raman spectrometer for the 217-400nm spectral region. Review of Scientific Instruments. 1983;54(12):1657-62.
4. Copeland RA, Spiro TG. Ultraviolet Raman hypochromism of the tropomyosin amide modes: a new method for estimating .alpha.-helical content in proteins. Journal of the American Chemical Society. 1986;108(6):1281-5.
5. Fodor SPA, Rava RP, Hays TR, Spiro TG. Ultraviolet resonance Raman spectroscopy of the nucleotides with 266-, 240-, 218-, and 200-nm pulsed laser excitation. Journal of the American Chemical Society. 1985;107(6):1520-9.
6. Rava RP, Spiro TG. Selective enhancement of tyrosine and tryptophan resonance Raman spectra via ultraviolet laser excitation. Journal of the American Chemical Society. 1984;106(14):4062-4.
7. Balakrishnan G, Weeks CL, Ibrahim M, Soldatova AV, Spiro TG. Protein dynamics from time resolved UV Raman spectroscopy. Current Opinion in Structural Biology. 2008;18(5):623-9.
8. Sanchez KM, Neary TJ, Kim JE. Ultraviolet Resonance Raman Spectroscopy of Folded and Unfolded States of an Integral Membrane Protein. The Journal of Physical Chemistry B. 2008;112(31):9507-11.
9. Oladepo SA, Xiong K, Hong Z, Asher SA. Elucidating Peptide and Protein Structure and Dynamics: UV Resonance Raman Spectroscopy. The Journal of Physical Chemistry Letters. 2011;2(4):334-44.
10. Oladepo SA, Xiong K, Hong Z, Asher SA, Handen J, Lednev IK. UV Resonance Raman Investigations of Peptide and Protein Structure and Dynamics. Chemical Reviews. 2012;112(5):2604-28.
11. Johnson CR, Asher SA. A new selective technique for characterization of polycyclic aromatic hydrocarbons in complex samples: UV resonance Raman spectrometry of coal liquids. Analytical Chemistry. 1984;56(12):2258-61.
12. Holtz JSW, Bormett RW, Chi Z, Cho N, Chen XG, Pajcini V, et al. Applications of a New 206.5-nm Continuous-Wave Laser Source: UV Raman Determination of Protein Secondary Structure and CVD Diamond Material Properties. Applied Spectroscopy. 1996;50(11):1459-68.

13. Gares KL, Bykov SV, Godugu B, Asher SA. Solution and Solid Trinitrotoluene (TNT) Photochemistry: Persistence of TNT-like Ultraviolet (UV) Resonance Raman Bands. Applied Spectroscopy. 2014;68(1):49-56.
14. Comanescu G, Manka CK, Grun J, Nikitin S, Zabetakis D. Identification of Explosives with Two-Dimensional Ultraviolet Resonance Raman Spectroscopy. Applied Spectroscopy. 2008;62(8):833-9.
15. López-Díez EC, Goodacre R. Characterization of Microorganisms Using UV Resonance Raman Spectroscopy and Chemometrics. Analytical Chemistry. 2003;76(3):585-91.
16. Jarvis RM, Goodacre R. Ultra-violet resonance Raman spectroscopy for the rapid discrimination of urinary tract infection bacteria. FEMS Microbiology Letters. 2004;232(2):127-32.
17. Asher SA, Mikhonin AV, Bykov S. UV Raman Demonstrates that α-Helical Polyalanine Peptides Melt to Polyproline II Conformations. Journal of the American Chemical Society. 2004;126(27):8433-40.
18. Mikhonin AV, Bykov SV, Myshakina NS, Asher SA. Peptide Secondary Structure Folding Reaction Coordinate: Correlation between UV Raman Amide III Frequency, Ψ Ramachandran Angle, and Hydrogen Bonding. The Journal of Physical Chemistry B. 2006;110(4):1928-43.
19. Huang C-Y, Balakrishnan G, Spiro TG. Protein secondary structure from deep-UV resonance Raman spectroscopy. Journal of Raman Spectroscopy. 2006;37(1-3):277-82.
20. Chi Z, Chen XG, Holtz JSW, Asher SA. UV Resonance Raman-Selective Amide Vibrational Enhancement: Quantitative Methodology for Determining Protein Secondary Structure. Biochemistry. 1998;37(9):2854-64.
21. Asher SA, Ianoul A, Mix G, Boyden MN, Karnoup A, Diem M, et al. Dihedral Ψ Angle Dependence of the Amide III Vibration: A Uniquely Sensitive UV Resonance Raman Secondary Structural Probe. Journal of the American Chemical Society. 2001;123(47):11775-81.
22. Mikhonin AV, Ahmed Z, Ianoul A, Asher SA. Assignments and Conformational Dependencies of the Amide III Peptide Backbone UV Resonance Raman Bands. The Journal of Physical Chemistry B. 2004;108(49):19020-8.
23. Mikhonin AV, Asher SA. Direct UV Raman Monitoring of 3_{10}-Helix and π-Bulge Premelting during α-Helix Unfolding. Journal of the American Chemical Society. 2006;128(42):13789-95.
24. Benevides JM, Overman SA, Thomas GJ. Raman, polarized Raman and ultraviolet resonance Raman spectroscopy of nucleic acids and their complexes. Journal of Raman Spectroscopy. 2005;36(4):279-99.
25. Thomas GJ. RAMAN SPECTROSCOPY OF PROTEIN AND NUCLEIC ACID ASSEMBLIES. Annual Review of Biophysics and Biomolecular Structure. 1999;28(1):1-27.
26. Huang C-Y, Balakrishnan G, Spiro TG. Early Events in Apomyoglobin Unfolding Probed by Laser T-jump/UV Resonance Raman Spectroscopy. Biochemistry. 2005;44(48):15734-42.
27. Mikhonin AV, Asher SA, Bykov SV, Murza A. UV Raman Spatially Resolved Melting Dynamics of Isotopically Labeled Polyalanyl Peptide: Slow α-Helix Melting Follows 3_{10}-Helices and π-Bulges Premelting. The Journal of Physical Chemistry B. 2007;111(12):3280-92.
28. Sanchez KM, Kang G, Wu B, Kim JE. Tryptophan-Lipid Interactions in Membrane Protein Folding Probed by Ultraviolet Resonance Raman and Fluorescence Spectroscopy. Biophysical Journal. 2011;100(9):2121-30.

29. Schlamadinger DE, Gable JE, Kim JE. Hydrogen Bonding and Solvent Polarity Markers in the UV Resonance Raman Spectrum of Tryptophan: Application to Membrane Proteins. The Journal of Physical Chemistry B. 2009;113(44):14769-78.
30. Shafaat HS, Sanchez KM, Neary TJ, Kim JE. Ultraviolet resonance Raman spectroscopy of a β-sheet peptide: a model for membrane protein folding. Journal of Raman Spectroscopy. 2009;40(8):1060-4.
31. Takeuchi H. Raman structural markers of tryptophan and histidine side chains in proteins. Biopolymers. 2003;72(5):305-17.
32. Takeuchi H. Raman spectral marker of tryptophan conformation: Theoretical basis and extension to a wider range of torsional angle. Journal of Molecular Structure. 2012;1023(0):143-8.
33. Hong Z, Wert J, Asher SA. UV Resonance Raman and DFT Studies of Arginine Side Chains in Peptides: Insights into Arginine Hydration. The Journal of Physical Chemistry B. 2013;117(24):7145-56.
34. Bykov SV, Sharma B, Asher SA. High-Throughput, High-Resolution Echelle Deep-UV Raman Spectrometer. Applied Spectroscopy. 2013;67(8):873-83.
35. Balakrishnan G, Hu Y, Nielsen SBn, Spiro TG. Tunable kHz Deep Ultraviolet (193-210 nm) Laser for Raman Application. Applied Spectroscopy. 2005;59(6):776-81.
36. Kaminaka S, Mathies RA. High-Throughput Large-Aperture Prism Prefilter for Ultraviolet Resonance Raman Spectroscopy. Applied Spectroscopy. 1998;52(3):469-73.
37. Oladepo SA, Loppnow GR. Initial Excited-State Structural Dynamics of 9-Methyladenine from UV Resonance Raman Spectroscopy. The Journal of Physical Chemistry B. 2011;115(19):6149-56.
38. Bykov S, Lednev I, Ianoul A, Mikhonin A, Munro C, Asher SA. Steady-State and Transient Ultraviolet Resonance Raman Spectrometer for the 193-270 nm Spectral Region. Appl Spectrosc. 2005;59(12):1541-52.
39. Grum F, Luckey GW. Optical Sphere Paint and a Working Standard of Reflectance. Appl Opt. 1968;7(11):2289-94.
40. Manka CK, Nikitin S, Lunsford R, Kunapareddy P, Grun J. Wavelength-dependent amplitude of Teflon Raman lines. Journal of Raman Spectroscopy. 2011;42(4):685-90.
41. Woutersen S, Hamm P. Structure Determination of Trialanine in Water Using Polarization Sensitive Two-Dimensional Vibrational Spectroscopy. The Journal of Physical Chemistry B. 2000;104(47):11316-20.
42. Sharma B, Asher SA. UV Resonance Raman Investigation of the Conformations and Lowest Energy Allowed Electronic Excited States of Tri- and Tetraalanine: Charge Transfer Transitions. The Journal of Physical Chemistry B. 2010;114(19):6661-8.
43. T. Shimanouchi, "Molecular Vibrational Frequencies" in **NIST Chemistry WebBook, NIST Standard Reference Database Number 69**, Eds. P.J. Linstrom and W.G. Mallard, National Institute of Standards and Technology, Gaithersburg MD, 20899, http://webbook.nist.gov, (retrieved April 17, 2014).